Ultra broadband flat dispersion tailoring on reversed-rib chalcogenide glass waveguide*

Yanfen Zhai(翟彦芬), Renduo Qi(齐人铎), Chenzhi Yuan(袁晨智), Wei Zhang(张巍)†, and Yidong Huang(黄翊东)

Tsinghua National Laboratory for Information Science and Technology, Department of Electronic Engineering, Tsinghua University, Beijing 100084, *China*

(Received 17 February 2016; revised manuscript received 12 May 2016; published online 30 September 2016)

In this paper, we introduce a horizontal slot in the reversed-rib chalcogenide glass waveguide to tailor its dispersion characteristics. The waveguide exhibits a flat and low dispersion over a wavelength range of 1080 nm, in which the dispersion fluctuates between -10.6 ps·nm^{-1}·km^{-1} and $+11.14$ ps·nm^{-1}·km^{-1}. The dispersion tailoring effect is due to the mode field transfer from the reversed-rib waveguide to the slot with the increase of wavelength, which results in the extension of the low dispersion band. Moreover, the nonlinear coefficient and the phase-matching condition of the four-wave mixing process in this waveguide are studied, showing that the waveguide has great potential in nonlinear optical applications over a wide wavelength range.

Keywords: chalcogenides films, nonlinear optics, waveguides, dispersion

PACS: 42.65.Wi, 42.65.–k, 42.79.–e, 77.84.Bw **DOI:** 10.1088/1674-1056/25/11/114211

1. Introduction

Chromatic dispersion is an essential property of nonlinear waveguides, which plays a critical role in many nonlinear processes, such as soliton formation,[1–6] supercontinuum generation,[3,7–10] four-wave-mixing (FWM) based amplification,[11] and wavelength conversion.[12–16] Low and flat dispersion over a broad wavelength range is preferred for optimizing the phase matching condition.[17] Recently, chalcogenide glass (ChG) waveguides have drawn much attention as promising candidates for integrated nonlinear photonic devices.[18–29] Many ChG materials have high Kerr nonlinear indexes (n_2) and low two-photon absorption coefficients;[30–32] hence, they have high figure of merit (FOM) of the third-order nonlinear optical materials.[30,31] However, ChG materials usually have large negative dispersion at the near-infrared and mid-infrared bands, which requires a special waveguide design to compensate for the material dispersion by the waveguide dispersion.[17,22,23,33–37]

Strip and rib waveguides are the most popular structures of ChG waveguides. The geometry parameters of these structures can be adjusted to tailor the waveguide dispersions. However, the bandwidth of low dispersion region is always limited. The introduction of a slot structure into the waveguide has been proven as an effective way to tailor the waveguide dispersion.[12,23,38–42] Recently, a strip/slot hybrid As_2S_3 waveguide design has been proposed, which has a flat dispersion band of 249 nm and whose dispersion is limited in ± 170 ps·nm^{-1}·km^{-1}.[43] Although this design shows impressive dispersion characteristics as nonlinear waveguides, many difficulties can be expected in its fabrication. On the one hand, the commercial (NH_4OH)-based developer using in the UV-lithography or electron beam lithography (EBL) may lead to pinholes and film peeling in ChGs[43–45] which impacts the quality of ChG waveguides. On the other hand, both the wet-etching and dry-etching processes on the ChG films are not easy due to the fragility of ChG materials.[27,45–49] Recently, we proposed a reverse ridge/slot hybrid As_2S_3 waveguide structure with an ultra-flat dispersion profile.[23] This structure can be fabricated by the micro-trench filling technique,[50] which avoids the photo lithography process, wet or dry etching processes and lift-off processes on the As_2S_3 layer. However, to realize this waveguide structure, vertical slot structures of tens of nanometers should be fabricated by dry etching on the silica substrate, and the requirement of the accuracy of the structure parameters is very high to realize dispersion flattening, which is difficult in waveguide fabrication.

In this paper, we introduce a horizontal slot in a reversed-rib As_2S_3 waveguide. This waveguide can also be fabricated by the micro-trench filling technique; however, the slot in the horizon direction replaces the vertical slots in the previous work[23] to tailor its dispersion property. Hence, the difficulties in the fabrication of the small slot structures in the silica substrate are avoided, leading to a simpler fabrication process. On the other hand, the dispersion of quasi-TM mode is adjusted by the horizontal slot in this structure, realizing an ultra-flat dispersion profile, which varies from -10.6 ps·nm^{-1}·km^{-1} to $+11.14$ ps·nm^{-1}·km^{-1} over a wavelength range of 1080 nm (from 1760 nm to 2840 nm).

*Project supported by the National Basic Research Program of China (Grant Nos. 2013CB328700 and 2011CBA00303) and the National Natural Science Foundation of China (Grant Nos. 61575102 and 61321004).

†Corresponding author. E-mail: zwei@tsinghua.edu.cn

2. Waveguide design and dispersion tailoring by the slot structure

Figure 1(a) shows the reversed-rib waveguide structure. Due to the low transformation temperature of As_2S_3,[28,31] the fabrication process of this structure is relatively simple. Firstly, a groove was made on the silica substrate by wet etching or dry etching. Secondly, the As_2S_3 film was deposited by traditional vacuum deposition methods (thermal evaporation, chemical vapor deposition or sputtering). Then, the sample was annealed to melt the As_2S_3 material, which made the upper surface of the film flat to realize the reversed-rib structure. It can also be fabricated by the micro-trench filling method based on solution-processed ChG.[27,29,51] Finally, a silica layer as the cladding of the waveguide could be fabricated by sputtering or the method based on the silicon based polymer. In this process, there is no photolithography or etch processes on the As_2S_3 film, which reduces the difficulty in the fabrication of ChG waveguides. It is worth noting that this structure can also be fabricated by the traditional top-down method, in which the ChG glass and silica materials are deposited layer by layer firstly, and then only the last ChG layer needs to be etched to form the ridge structure.

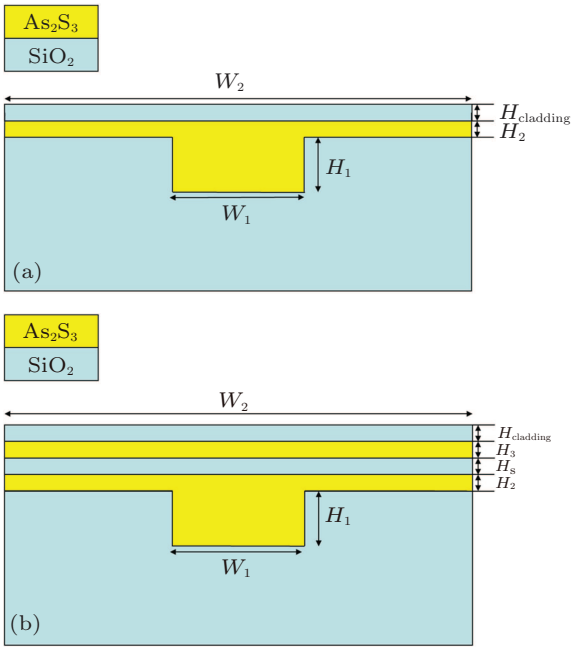

Fig. 1. Sketches of the proposed waveguide structures. (a) The reversed-rib waveguide without slot. (b) The reversed-rib waveguide with a silica slot.

To tailor the dispersion of the reversed-rib waveguide, we introduce a horizon slot above the rib, which is shown in Fig. 1(b). It can be realized by simply repeating the deposition of both As_2S_3 film and silica layer one more time.

Dispersion tailoring is carried out by properly optimizing the structural parameters of the waveguide including the rib width (W_1), the rib height (H_1), and the thicknesses of the As_2S_3 layer on the subtract (H_2), the silica slot (H_s), and the As_2S_3 layer above the slot (H_3). In order to prevent the oxidation of the ChG glass, the waveguide is covered with a layer of SiO_2 with a thickness of $H_{cladding}$. In this paper, the effective indexes (n_{eff}) of the fundamental quasi-TE mode and quasi-TM mode with different wavelengths are calculated by the finite-element mode method. In the calculation, the material dispersions of As_2S_3[52] and silica[53] are taken into account using their Sellmeier equations. The dispersion can be calculated by

$$D = -(\lambda/c)\left(\partial^2 n_{\text{eff}}/\partial\lambda^2\right), \tag{1}$$

where c and λ are the speed of light and the wavelength in vacuum, respectively. Figure 2 shows the dispersions of the fundamentalquasi-TE/TM modes in the waveguides shown in Fig. 1. The dashed-dotted blue line in Fig. 2 is the material dispersion of the As_2S_3. The red and black dashed lines are the dispersion of the fundamental quasi-TE and TM modes in the reversed-rib waveguide without slot (as shown in Fig. 1(a)). Here, the width and height of the rib are $W_1 = 1400$ nm and $H_1 = 714$ nm, respectively. The thicknesses of the As_2S_3 layer above the substrate (H_2) and the silica cladding layer ($H_{cladding}$) are 80 nm and 180 nm, respectively. Calculations show that no higher-order mode is supported under these structure parameters, except for the fundamental quasi-TE/TM modes. It can be seen that both modes have parabola-like dispersion curves with two zero dispersion wavelengths (ZDWs). The maximums of the dispersions of the quasi-TE and TM mode are close to 200 ps·nm^{-1}·km^{-1} and 320 ps·nm^{-1}·km^{-1}, respectively. Besides, it can be seen that the near-zero dispersion bands are all narrow near the ZDWs of the two modes in this waveguide.

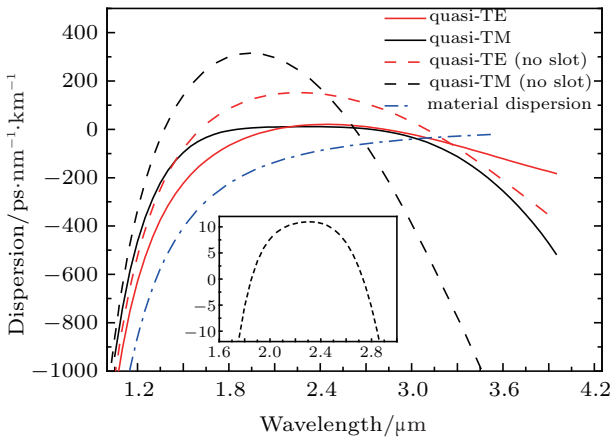

Fig. 2. Dispersion of the fundamental quasi-TE and quasi-TM modes in the reversed-rib waveguide with/without the slot. The solid red and black lines are the dispersion of the quasi-TE and quasi-TM modes in the reversed-rib waveguide with a slot, respectively. The dashed red and black lines are the dispersion of the quasi-TE and quasi-TM modes in the reversed-rib waveguide without slot, respectively. The blue dashed-dotted line is the material dispersion of the As_2S_3.

The red and black solid lines in Fig. 2 are the dispersion of the fundamental quasi-TE and -TM modes in the reversed-rib waveguide with the slot (as shown in Fig. 1(b)). Here, the width and height of the rib (W_1, H_1), the thickness of the As_2S_3 layer above the substrate (H_2), and the silica cladding layer ($H_{cladding}$) are all the same as those of the waveguide without the slot. The thicknesses of the silica slot (H_s) and the As_2S_3 layer above the slot (H_3) are 93 nm and 230 nm, respectively. It can be seen that, for both modes, the dispersion shows flatter profiles with broader near-zero dispersion bands than that of the reversed-rib waveguide without the slot. The inset of Fig. 2 shows the detail of the dispersion of the quasi-TM mode in the reversed-rib waveguide with the slot. It can be seen that it has two ZDWs at 1849 nm and 2742 nm, respectively. The dispersion is limited between -10.6 ps·nm^{-1}·km^{-1} and $+11.14$ ps·nm^{-1}·km^{-1} over a band of 1080 nm (from 1760 nm to 2840 nm).

To show the mechanism of the dispersion tailoring effect of the silica slot, the electric field distributions of the quasi-TM modes with different wavelengths in the proposed waveguide with slots and without slots are calculated and shown in Figs. 3(a) and 3(b), respectively. It can be seen that the electric field concentrates in the rib region at the short wavelength. As the wavelength increases, the electric field gradually transfers into the SiO_2 slot. This mode field transfer provides a modification on the waveguide dispersion of the reversed-rib waveguide. Hence, the slot provides additional dispersion tailoring freedom.

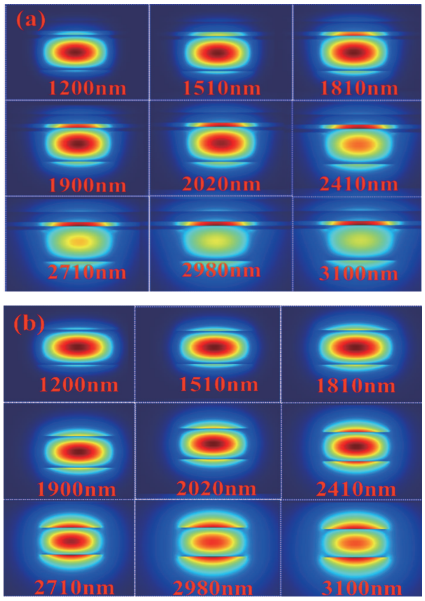

Fig. 3. Quasi-TM mode evolution of the waveguide for various wavelengths (a) with slots and (b) without slots.

3. The influence of structure parameters on the dispersion property

The slot structure provides enough degrees of freedom to tailor the waveguide dispersion. On the other hand, the variation of structure parameters, which is unavoidable in waveguide fabrication, would also impact the dispersion property of the waveguide. Figure 4 shows the influence of structural parameters on the dispersion of the fundamental quasi-TM mode by changing them around the optimized values.

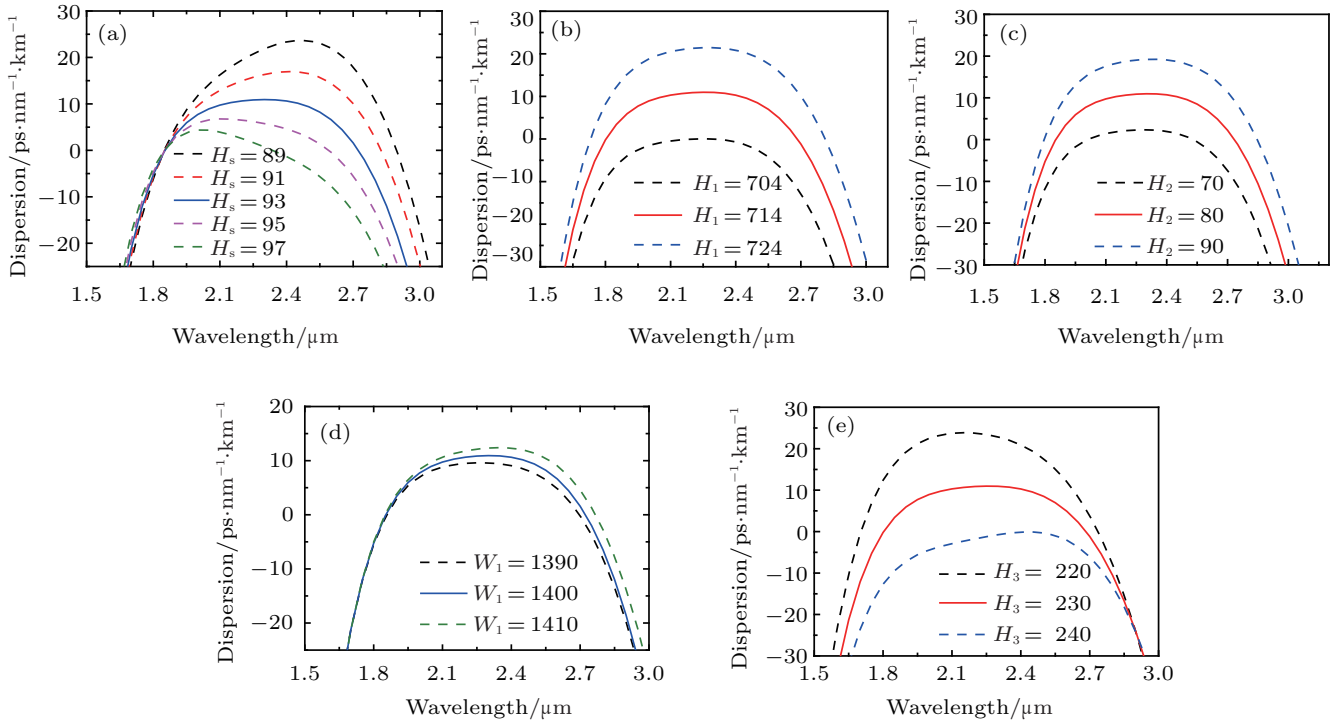

Fig. 4. Dispersion profiles of the slot waveguides with different (a) slot thicknesses (H_s), (b) heights of groove (H_1), (c) heights of the As_2S_3 layer (H_2), (d) widths of groove (W_1), and (e) heights of another As_2S_3 layer (H_3).

Figure 4(a) shows the calculation results of dispersion with different thicknesses of the slot. The other structure parameters used in this calculation are the same as the optimized design used in Fig. 2 (This condition is also used in the calculations of Figs. 4(b)–4(e)). It can be seen that the dispersion curve with a larger slot thickness shows higher suppression at the long-wavelength band. By optimizing the slot parameters, a dispersion curve with a flat profile can be realized.

The dispersion profiles for different rib heights (H_1) are plotted in Fig. 4(b). It can be seen that the dispersion profile is almost unchanged. While it rises as a whole as H_1 increases from 704 nm to 724 nm, the maximum dispersion value rises from 0 ps·nm^{-1}·km^{-1} to 21.43 ps·nm^{-1}·km^{-1}, with a rate about 1 ps·nm^{-1}·km^{-1} per nanometer. A similar effect can be seen when the thickness of the As_2S_3 layer on the subtract (H_2) changes. Figure 4(d) shows the calculation results under different rib widths (W_1). When the width varies from 1390 nm to 1410 nm, the dispersion shape and slope at the short wavelength are almost unchanged. However, the dispersion in the longer wavelength region changes rapidly and the dispersion on the peak increases from 9.5 ps·nm^{-1}·km^{-1} to 12.4 ps·nm^{-1}·km^{-1} with a rate about 0.15 ps·nm^{-1}·km^{-1} per nanometer.

The influence of the thickness of the As_2S_3 layer above the slot (H_3) is calculated and shown in Fig. 4(e). The dispersion profile drops with the increase of H_3. The maximum dispersion reduces with a rate of about 1 ps·nm^{-1}·km^{-1} per nanometer and shifts to longer wavelength.

By comparing the results in Fig. 4, it can be seen that the slot thickness is the most sensitive structure parameter for the dispersion profile. Hence, its fine control in the fabrication process is the key to obtain a flat and near-zero dispersion profile.

4. The performance of the proposed waveguide as a third-order nonlinear waveguide

The As_2S_3 glass has the third-order nonlinear index (n_2) of 2.92×10^{-18} m^2/W and a low TPA coefficient of 6.2×10^{-15} m/W at the telecom band. Its nonlinear FOM is as high as 312, which is much higher than that of the silicon waveguide (0.77).[31] On the other hand, the proposed waveguide structure provides an effective way to realize a flat dispersion profile, which is preferred in many third-order parametric nonlinear processes. Hence, the proposed waveguide has great potential as a nonlinear medium for developing integrated nonlinear devices. To show this more clearly, we calculated the third-order nonlinear coefficient of the fundamental quasi-TM modes in the proposed waveguide with different wavelengths by

$$\gamma_e = \frac{2\pi}{\lambda}\frac{\iint_{-\infty}^{\infty} n_2(x,y)\,|F(x,y)|^4\,\mathrm{d}x\mathrm{d}y}{\left(\iint_{-\infty}^{\infty}|F(x,y)|^2\,\mathrm{d}x\mathrm{d}y\right)^2}, \tag{2}$$

where $F(x,y)$ is the distribution of the electric field and is the light wavelength, A_{eff} is the effective area of the mode, which is calculated by[54]

$$A_{\mathrm{eff}} = \frac{\left(\iint_{-\infty}^{\infty}|F(x,y)|^2\,\mathrm{d}x\mathrm{d}y\right)^2}{\iint_{-\infty}^{\infty}|F(x,y)|^4\,\mathrm{d}x\mathrm{d}y}. \tag{3}$$

The structure parameters used here are the same as those used in Fig. 2, in which quasi-TM mode of the proposed waveguide has an ultra-flat profile with a broad near zero dispersion band. Figure 5 shows the calculated (blue circles) and (black squares), respectively. It can be seen that, as the wavelength increases, the effective area of the mode increases while the nonlinear coefficient reduces. At a short wavelength, most of the electric field is confined in the reversed-rib of the As_2S_3 waveguide. As the wavelength increases, the electric field increasingly extends to the silica slot. Hence, the nonlinear coefficient gradually decreases due to the electric field extension into the silica slot with a lower nonlinear index.

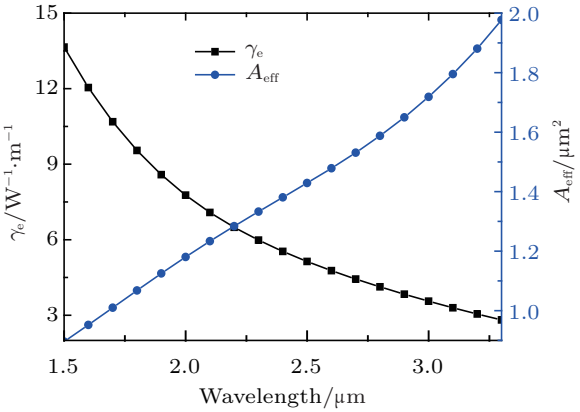

Fig. 5. (color online) The effective area A_{eff} (blue circles) and the nonlinear coefficient γ_e (black squares) of the fundamental quasi-TM mode in the proposed reversed-rib waveguide with a slot. The structure parameters used in the calculation are the same as those used in Fig. 2.

To demonstrate the potential of this waveguide in the third-order parametric processes, we calculated the linear phase mismatching of the degenerate four-wave mixing by $\Delta\beta = \beta_s + \beta_i - 2\beta_p$, where β_s, β_i, and β_p are propagation constants of the signal, idler, and pump lights, respectively. The quasi-TM mode with the ultra-flat profile is considered in this calculation. The calculation results are shown in Fig. 6. Figure 6(a) is the linear phase mismatching under different pump wavelengths λ_{pump} and signal-pump wavelength differences Δ_λ. Different colors in the figure represent the values of linear phase mismatching under different λ_{pump} and differences Δ_λ. It can be seen that if the pump light is set close to the two ZDWs, small linear phase mismatching could be realized over large regions of signal-pump wavelength difference Δ_λ.

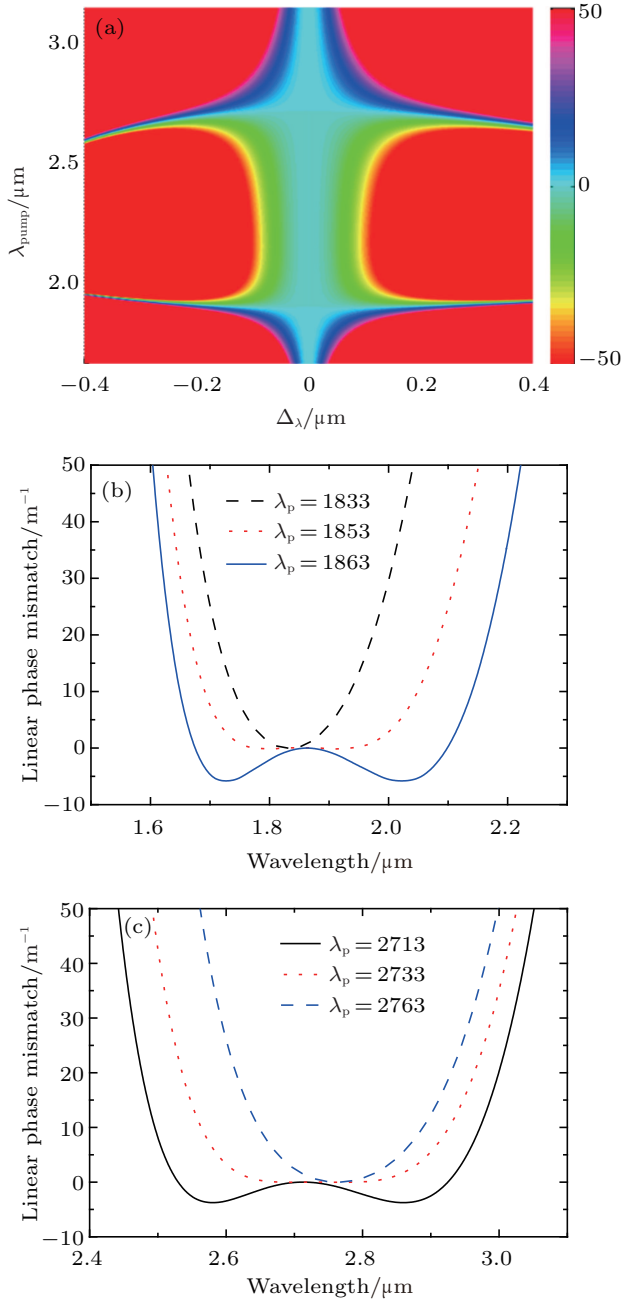

Fig. 6. Calculation results of linear phase mismatching of the degenerate FWM process in this waveguide. (a) Linear phase mismatching $\Delta\beta$ under different pump wavelengths and signal-pump wavelength differences Δ_λ, (b) linear phase mismatching under different signal wavelengths when the pump wavelength is set near the shorter ZDW, (c) linear phase mismatching under different signal wavelengths when the pump wavelength is set near the longer ZDW.

To show this more clearly, the linear phase mismatch profiles when the pump wavelength is set near the shorter ZDW (1849 nm) and longer ZDW (2742 nm) are plotted in Figs. 6(b) and 6(c), respectively. It can be seen that when pump wavelength is set to 1853 nm, which is close to the shorter ZDW (1849 nm), the linear phase mismatching profile is like an upward parabola with a zero point at $\Delta_\lambda = 0$ and a broad near-zero band. When the pump wavelength decreases, e.g., to 1833 nm, the parabola-like profile shrinks, leading to a smaller near-zero band. On the other hand, when the pump wavelength increases, e.g., to 1863 nm, two regions with negative linear phase mismatching appear at two sides, which would be deeper and wider if the pump wavelength increases further. The profile of the linear phase mismatching when the pump light is near the longer ZDW (2742 nm) is similar with the case that it is near the shorter ZDW. However, its variation with the pump wavelength is different. It can be seen that the two regions with negative linear phase mismatching appear when the pump wavelength is shorter than the longer ZDW, with a broader near-zero band.

It is well known that a small negative linear mismatching is preferred to the degenerate fourwave mixing because it can be compensated by the nonlinear mismatching term under a proper pump level. Hence, to realize the broad band degenerate fourwave mixing in the quasi-TM mode of the proposed waveguide, the pump light should have a wavelength a little longer than the shorter ZDW or a little shorter than the longer ZDW.

5. Conclusion

In this paper, we proposed a reversed-rib As_2S_3 waveguide with a slot to tailor its dispersion. By properly designing its structure parameters, an ultra-flat and near zero dispersion profile can be realized, in which the dispersion is limited between -10.6 ps·nm^{-1}·km^{-1} and $+11.14$ ps·nm^{-1}·km^{-1} over a band of 1080 nm. The slot structure provides a dispersion tailing effect to extend the low dispersion band, which is due to the electric field transfer process from the reversed-rib waveguide to the slot as the wavelength increases. To demonstrate its potential as a nonlinear waveguide for integrated nonlinear optical devices, its nonlinear coefficient and the linear phase mismatching profile for the degenerate FWM are also calculated, showing that the waveguide can support broadband degenerate FWM in near infrared and middle infrared band if the pump wavelength is set a little longer than the shorter ZDW or a little shorter than the longer ZDW. The proposed As_2S_3 waveguide can be fabricated without photolithography and etching processes on the As_2S_3 film, which can reduce the difficulty in the fabrication of ChG waveguides, showing great potential in applications of nonlinear photonic devices.

References

[1] Chavez B J M, Bodenmüller D, Fremberg T, Haynes R, Roth M M, Eisermann R, Lisker M, Zimmermann L and Böhm M 2014 *J. Opt. Soc. Am. B* **31** 2846
[2] Lamont M R, Luther-Davies B, Choi D Y, Madden S and Eggleton B J 2008 *Opt. Express* **16** 14938
[3] De Leonardis F and Passaro V M N 2011 *Adv. Optoelectron.* **2011** 751498
[4] Duan L, Yang Z Y, Liu C and Yang W L 2016 *Chin. Phys. Lett.* **33** 10501
[5] Wang H Y, Xu W C, Luo Z C, Luo A P, Cao W J, Dong J L and Wang L Y 2011 *Chin. Phys. Lett.* **28** 024207

[6] Amiri I S, Afroozeh A, Bahadoran M, Amiri I S, Afroozeh A and Bahadoran M 2011 *Chin. Phys. Lett.* **28** 104205

[7] McCarthy J, Bookey H, Beecher S, Lamb R, Elder I and Kar A K 2013 *Appl. Phys. Lett.* **103** 151103

[8] Zhang H, Das S, Huang Y, Li C, Chen S, Zhou H, Yu M, Guo-Qiang L P and Thong J T L 2012 *Appl. Phys. Lett.* **101** 021105

[9] Yu Y, Gai X, Wang T, Ma P, Wang R, Yang Z, Choi D Y, Madden S and Luther-Davies B 2013 *Opt. Mater. Express* **3** 1075

[10] Zhang L, Lin Q, Yue Y, Yan Y, Beausoleil R G and Willner A E 2012 *Opt. Express* **20** 1685

[11] Liang T K and Tsang H K 2004 *Appl. Phys. Lett.* **84** 2745

[12] Liu Q, Gao S, Li Z, Xie Y and He S 2011 *Appl. Opt.* **50** 1260

[13] Lin Q, Zhang J, Fauchet P M and Agrawal G P 2006 *Opt. Express* **14** 4786

[14] Lamont M R, de Sterke C M and Eggleton B J 2007 *Opt. Express* **15** 9458

[15] An L, Liu H, Sun Q, Huang N and Wang Z 2014 *Appl. Opt.* **53** 4886

[16] Jin B, Yuan J, Yu C, Sang X, Wei S, Zhang X, Wu Q and Farrell G 2014 *Opt. Express* **22** 6257

[17] Collins M J, Clark A S, He J, Choi D Y, Williams R J, Judge A C, Madden S J, Withford M J, Steel M J, Luther-Davies B, Xiong C and Eggleton B J 2012 *Opt. Lett.* **37** 3393

[18] Cardinal T, Richardson K A, Shim H, Schulte A, Beatty R, Le Foulgoc K, Meneghini C, Viens J F and Villeneuve A 1999 *J. Non-Cryst. Solids* **256** 353

[19] Viens J F, Meneghini C, Villeneuve A, Galstian T V, Knystautas E J, Duguay M A, Richardson K A and Cardinal T 1999 *J. Light. Technol.* **17** 1184

[20] Feigel A, Kotler Z, Sfez B, Arsh A, Klebanov M and Lyubin V 2000 *Appl. Phys. Lett.* **77** 3221

[21] Zhai Y, Qi R, Yuan C, Dong S, Zhang W and Huang Y 2016 *IEEE Photonics J.* **8** 2700709

[22] Al-Kadry A, Li L, Amraoui M E, North T, Messaddeq Y and Rochette M 2015 *Opt. Lett.* **40** 4687

[23] Zhai Y, Yuan C, Qi R, Zhang W and Huang Y 2015 *IEEE Photonics J.* **7** 7801609

[24] Chiles J, Malinowski M, Rao A, Novak S, Richardson K and Fathpour S 2015 *Appl. Phys. Lett.* **106** 111110

[25] Luther-Davies B, Yu Y, Zhang B, Gai X, Zhai C, Qi S, Guo W, Yang Z, Wang R, Choi D Y, Madden S, Moller U, Kubat I, Petersen C, Brilland L, M'echin D, Caillaud C, Troles J and Bang O 2015 *Nonlinear Optics* 2015*, OSA Technical Digest* p. NTu1A.4

[26] Yu Y, Gai X, Ma P, Choi D Y, Yang Z, Wang R, Debbarma S, Madden S J and Luther-Davies B 2014 *Laser Photonics Rev.* **8** 792

[27] Zou Y, Moreel L, Lin H, Zhou J, Li L, Danto S, Musgraves J D, Koontz E, Richardson K, Dobson K D, Birkmire R and Hu J 2014 *Adv. Opt. Mater.* **2** 759

[28] Zou Y, Zhang D, Lin H, Li L, Moreel L, Zhou J, Du Q, Ogbuu O, Danto S, Musgraves J D, Richardson K, Dobson K D, Birkmire R and Hu J 2014 *Adv. Opt. Mater.* **2** 478

[29] Zha Y, Lin P T, Kimerling L, Agarwal A and Arnold C B 2014 *ACS Photonics* **1** 153

[30] Gai X, Madden S, Choi D Y, Bulla D and Luther-Davies B 2010 *Opt. Express* **18** 18866

[31] Eggleton B J, Luther-Davies B and Richardson K 2011 *Nat. Photonics* **5** 141

[32] Eggleton B J 2010 *Opt. Express* **18** 26632

[33] Karim M R, Rahman B M A, Azabi Y O, Agrawal A and Agrawal G P 2015 *JOSA B* **32** 2343

[34] Luther-Davies B, Gai X, Madden S J, Choi D Y, Yang Z, Wang R, Ma P and Yu I 2013 *CLEO: Science and Innovations* (Optical Society of America) p. CM1L

[35] Eggleton B J, Vo T D, Pant R, Schr J, Pelusi M D, Yong C D, Madden S J and Luther-Davies B 2012 *Laser Photonics Rev.* **6** 97

[36] Collins M J, Clark A, He J, Shahnia S, Williams R J, Judge A C, Magi E, Choi D Y, Luther-Davies B and Eggleton B J 2012 *Frontiers in Optics* (Optical Society of America) p. FTu4D

[37] Qiao H A, Anheier N C, Musgrave J D, Richardson K and Hewak D W 2011 *SPIE Defense, Security, and Sensing* (International Society for Optics and Photonics) p. 80160F

[38] Bao C, Yan Y, Zhang L, Yue Y, Ahmed N, Agarwal A M, Kimerling L C, Michel J and WillnerA E 2015 *J. Opt. Soc. Am. B* **32** 26

[39] Liu Y, Yan J and Han G 2014 *Appl. Opt.* **53** 6302

[40] Wang S, Hu J, Guo H and Zeng X 2013 *Opt. Express* **21** 3067

[41] Nolte P W, Bohley C and Schilling J 2013 *Opt. Express* **21** 1741

[42] Zhu M, Liu H, Li X, Huang N, Sun Q, Wen J and Wang Z 2012 *Opt. Express* **20** 15899

[43] Zhang L, Yue Y, Xiao-Li Y, Wang J, Beausoleil R G and WillnerA E 2010 *Opt. Express* **18** 13187

[44] He J, Xiong C, Clark A S, Collins M J, Gai X, Choi D Y, Madden S J, Luther-Davies B and Eggleton B J 2012 *J. Appl. Phys.* **112** 123101

[45] Choi D Y, Maden S, Rode A, Wang R and Luther-Davies B 2008 *J. Non-Cryst. Solids* **354** 3179

[46] Gai X, Han T, Prasad A, Madden S, Choi D Y, Wang R, Bulla D and Luther-Davies B 2010 *Opt. Express* **18** 26635

[47] Choi D Y, Madden S, Rode A, Wang R, Bulla D and Luther-Davies B 2008 *J. Non-Cryst. Solids* **354** 5253

[48] Choi D Y, Madden S, Bulla D A, Wang R, Rode A and Luther-Davies B 2010 *IEEE Photonics Technol. Lett.* **22** 495

[49] Pittman T B, Jacobs B C and Franson J D 2005 *Opt. Commun.* **246** 545

[50] Zhai Y, Qi R, Yuan C, Zhang W and Huang Y 2016 *Appl. Phys. Express* **9** 052201

[51] Barile C J, Nuzzo R G and Gewirth A A 2015 *J. Phys. Chem. C* **119** 13524

[52] Rodney W S, *et al.* 1958 *Anon Refractive Index of* As_2S_3 *(Arsenic Trisulfide)*

[53] Malitson I H 1965 *Anon Refractive Index of* SiO_2 *(Silicon Dioxide, Silica, Quartz)*

[54] Li L, Zou Y, Lin H, Hu J, Sun X, Feng N N, Danto S, Richardson K, Gu T and Haney M 2013 *J. Light. Technol.* **31** 4080